

Study of the effect of dopant concentration on the optical uniformity and photorefractive properties of $\text{LiNbO}_3:\text{Er}:\text{Zn}$ single crystals

© I.V. Biryukova, R.A. Titov, N.A. Teplyakova, I.N. Efremov, M.N. Palatnikov

Tananaev Institute of Chemistry — Subdivision of the Federal Research Centre „Kola Science Centre of the Russian Academy of Sciences“,
184209 Apatity, Russia
e-mail: r.titov@ksc.ru

Received June 30, 2023

Revised August 29, 2023

Accepted September 9, 2023

The physicochemical characteristics, optical uniformity and photorefractive properties of a series of four $\text{LiNbO}_3:\text{Er}:\text{Zn}$ single crystals have been studied. Single crystals have been obtained by the Czochralski method. The erbium content in the crystals was ~ 0.5 mol.% and the zinc content in the crystals was $\sim 4.02, 4.41, 4.65, 4.66$ mol.%. The dopant distribution in the $\text{LiNbO}_3:\text{Er}:\text{Zn}$ melt–crystal system has been studied, and the optimal concentration ranges of erbium and zinc in the initial melt have been determined. The ranges provide crystals with high chemical, optical uniformity and resistance to optical damage for applications in optoelectronics and laser technology.

Keywords: lithium niobate, crystals, erbium, zinc, double doping, distribution coefficient, laser conoscopy, photoinduced light scattering.

DOI: 10.61011/TP.2023.11.57496.162-23

Introduction

Lithium niobate (LiNbO_3) single-crystals are constitute essential functional materials due to unique combination of their ferroelectric, pyroelectric and piezoelectric properties as well as to possible modification of beneficial properties by doping [1–7]. Modern applications of LiNbO_3 in non-linear, polarization and integrated optics, laser systems and optoelectronics require dramatically new approaches to the formation of development fundamentals for the Czochralski single crystal pulled-growth technology.

Creation of new lithium-niobate-based materials, that have high optical homogeneity and optical damage resistance, by doping method includes search for high performance methods of controlled exposure of a defect crystal structure. Thus, for example, introduction of pre-defined concentrations of non-photorefractive dopants (Mg, Zn, In, Sc, Gd, B) into the lithium niobate structure allows to improve considerably the crystal resistance to laser emission damage [3,8–14]. Such crystals also feature low coercive field and are promising optical materials for laser emission conversion, including periodically polarized domain structures [15].

Rare-earth-doped LiNbO_3 single crystals can induce laser oscillation on active rare earth ions with simultaneous self-doubling of laser emission frequency that is of great practical interest [16–21]. In particular, erbium-doped lithium niobate single crystals are used as active material for laser emission sources and signal amplifiers in fiber-optic communication lines. Unfortunately, photorefractive effect present in $\text{LiNbO}_3:\text{Er}$ crystals limits their application range [22,23]. In order to reduce the photorefractive effect

in $\text{LiNbO}_3:\text{Er}$ crystals, the use of non-photorefractive Zn^{2+} as the second dopant is more feasible than of Mg^{2+} , because $\text{LiNbO}_3:\text{Mg}$ crystals feature a „dark track“ effect [24] that results in reduction of visible spectrum transmittance by 10–15% [11]. Therefore, improvement of $\text{LiNbO}_3:\text{Er}$ single-crystal properties in order to increase optical homogeneity and optical damage resistance is possible with simultaneous introduction of erbium cations and zinc cations, as non-photorefractive dopant, into the lithium niobate structure [11,22,23,25–28].

Wide use of such material for mass production requires a reproducible technology for growing doped single crystals with high degree of chemical and optical homogeneity. Important research aspects include investigation of physical and chemical properties of the melt–crystal system, features of dopant distribution depending on thermal and process conditions of growing and on the best concentration of doping components in the melt that together have a complex impact on crystal composition, secondary (defect) structure and application properties.

The purpose of the study is to investigate distribution of doping components in the $\text{LiNbO}_3:\text{Er}:\text{Zn}$ melt–crystal system and to determine the best concentration ranges of Er and Zn in the melt for reproducible Czochralski growth of single crystals having high chemical and optical homogeneity and high laser damage resistance.

1. Experiment procedure

A combined doping method was used to grow a series of $\text{LiNbO}_3:\text{Er}:\text{Zn}$ single crystals. $\text{LiNbO}_3:\text{Er}$

charge made by solid-phase synthesis—granulation from $\text{Nb}_2\text{O}_5 + \text{Er}_2\text{O}_3 + \text{Li}_2\text{CO}_3$ mixture was used as the basis for growing a series of $\text{LiNbO}_3:\text{Er}:\text{Zn}$ single crystals. Erbium concentration in the charge according to the X-ray fluorescence spectrometry data was 0.93 wt.% (0.86 mol.% Er) [29]. Zinc was added to the melt and $\text{LiNbO}_3:\text{Er}$ charge in the form of pre-annealed Ultra High Pure ZnO in the concentration range 2.4–3.16 wt.% Zn. Doping was carried out from lower to higher concentration with an increment of 0.3 wt.% Zn. Concentration range was selected on the basis of previous comprehensive research of a series of $\text{LiNbO}_3:\text{Zn}$ single crystals grown from the melt with various zinc content (4.02–8.91 mol.%) [8,30] where optimum concentrations of dopant in the initial melt were determined to obtain single crystals with high chemical, optical and structural homogeneity and high laser damage resistance.

$\text{LiNbO}_3:\text{Er}:\text{Zn}$ single crystals 30 mm in diameter with a cylindrical section length of 30–35 mm were grown in direction (001) by the Czochralski method from 80 mm platinum crucibles in air [29]. To release thermoelastic stress, the grown single crystals were additionally annealed at $T = 1240^\circ\text{C}$ during 15 h in PVK-1.4-25 annealing furnace. To determine chemical homogeneity of the grown $\text{LiNbO}_3:\text{Er}:\text{Zn}$ crystals, 0.8 mm plates were cut from the cone and bottom sections of each ingot to measure Zn and Er concentrations in them. Erbium concentration was measured by the X-ray fluorescence spectrometry method („Spektroskan MAKSGV“), zinc concentration was measured by the atomic absorption spectrometry method („ANALYST-400“).

Crystals were brought into the single-domain state by the high temperature electrodiffusion annealing (HTEDA) method using DC current during cooling of samples in the temperature range 1232.5–742°C [29]. Unipolarity of $\text{LiNbO}_3:\text{Er}:\text{Zn}$ crystals was controlled by the static piezoelectric effect investigation method. Piezoelectric constant determination procedure (d_{333}) for a crystal ingot is described in [31].

Optical quality of the material was assessed by the number of scattering centers per unit volume of a single-crystal ingot according to the procedure described in [8]. The presence of scattering centers in the crystals was caused by structure defects and internal stresses induced by single crystal growth and post-treatment.

A laser conoscopy method was used to achieve large-scale conoscopic patterns [32]. Nd:YAG MLL-100 ($\lambda = 532.0$ nm, $P = 1$ and 90 mW) laser emission was used. Conoscopic samples consisted of polished 3 mm plates cut in direction (001). For the conoscopic test, the crystal sample was placed on a mobile two-axis optical support to allow full scanning of the input face plane by the laser beam and to get multiple conoscopic patterns corresponding to various areas on the test sample cross-section. Thus, optical homogeneity in the volume of the grown crystal was assessed. The test setup and procedure for recording

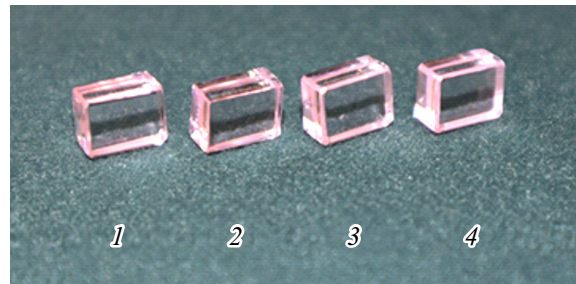


Figure 1. $\text{LiNbO}_3:\text{Er}:\text{Zn}$ (№1–4) single-crystal samples cut in the form of parallelepipeds.

conoscopic patterns in LiNbO_3 crystals are described in more detail in [32].

Samples for registration the photoinduced light scattering (PILS) were cut from $\text{LiNbO}_3:\text{Er}:\text{Zn}$ single crystals in the form of $8 \times 6 \times 4$ mm parallelepipeds whose edges coincided with crystal axis directions $X \times Y \times Z$, and faces were thoroughly polished (Figure 1). The PILS experiments used Nd:YAG MLL-100 ($\lambda = 532.0$ nm, $P = 160$ mW) laser. The test sample was placed on the laser beam path in such a way that the light wave vector is directed along the Y axis, normal to the input face of the crystal, and the electric field strength vector of the light wave E is parallel to the Z axis that coincides with the polar axis P_s of the lithium niobate crystal. The photorefraction effect for LiNbO_3 crystal is manifested most vividly in such scattering geometry. The test setup and procedure for determining the PILS indicatrix are described in detail in [32,33].

2. Findings and discussion

The first single crystal from the series was grown without zinc addition [29]. Then $\text{LiNbO}_3:\text{Er}:\text{Zn}$ with a weight of 122.8, 126.1, 124.1 and 130.5 g were grown in the same thermal and process conditions. Doped $\text{LiNbO}_3:\text{Er}$ charge and zinc oxide were added. Initial erbium concentration in the melt after growing the first $\text{LiNbO}_3:\text{Er}$ single crystal was equal to 0.79 mol.%. Zinc concentration was determined according to the first ZnO charge and was equal to 5.42 mol.%.

In order to study dopant distribution in the $\text{LiNbO}_3:\text{Er}:\text{Zn}$ melt–crystal system using the previous test data described in [29] regarding the dopant concentrations in grown single crystals and according to the procedure described in [8,30], initial concentrations of Er and Zn in the $\text{LiNbO}_3:\text{Er}:\text{Zn}$ melt for each single crystal growth, difference in the dopant concentration in the cone and bottom sections of single crystals (ΔC), and dopant distribution estimation coefficient ($K_{0\text{er}}$) characterizing the multicomponent system of interest were determined. The experimental and design data is provided in the Table.

The data in the Table demonstrates almost permanent concentrations of erbium and zinc along the growth axis of $\text{LiNbO}_3:\text{Er}:\text{Zn}$ single crystals grown

Dopant concentrations in the initial melt (C_{LZn} and C_{LEr} , mol.%), cone (C_{cone}) and bottom (C_{bott}) sections of the grown single crystals (C_{SZn} and C_{SEr}), $\Delta C = C_{cone} - C_{bott}$ and dopant distribution coefficients K_{0effZn} and K_{0effEr}

Single crystal No.	Concentration, mol.%						ΔC , mol.%		Distribution coefficient	
	In the melt		In the crystal				ΔC_{Zn}	ΔC_{Er}	K_{0effZn}	K_{0effEr}
	C_{LZn}	C_{LEr}	Cone		Bottom					
			C_{SZn}	C_{SEr}	C_{SZn}	C_{SEr}				
1	5.42	0.79	4.02	0.54	4.02	0.53	0	0.01	0.74	0.68
2	6.15	0.81	4.41	0.53	4.44	0.54	-0.03	-0.01	0.72	0.65
3	6.81	0.82	4.65	0.51	4.70	0.51	-0.05	0	0.68	0.62
4	6.98	0.85	4.66	0.50	4.68	0.50	-0.02	0	0.67	0.59

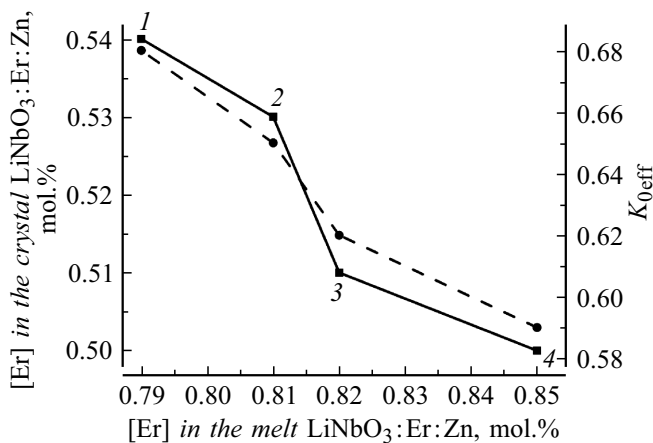


Figure 2. Dependences of Er concentration (solid line, squares) and estimation distribution coefficient K_{0effEr} (dashed line, circles) in $\text{LiNbO}_3:\text{Er}:\text{Zn}$ crystals on Er concentration in the melt. The numbers correspond to the single crystal Nos. (see the Table).

from the melt throughout the concentration range ($C_{Er} = 0.79\text{--}0.85$ mol.%, $C_{Zn} = 5.42\text{--}6.98$ mol.%). Difference in the concentration of doping components between the cone and bottom sections of $\text{LiNbO}_3:\text{Er}:\text{Zn}$ single crystals is max. 0.05 mol.% for zinc and max. 0.01 mol.% for erbium (see the Table). This is indicative of high degree of chemical homogeneity of $\text{LiNbO}_3:\text{Er}:\text{Zn}$ single crystals typical for crystals grown from melts with K_{0eff} close to unity. However, $K_{0eff} = C_S/C_L$, (where C_S is the dopant concentration in the cone section of the crystal, C_L is the dopant concentration in the melt) that governs the dopant distribution in the melt–crystal system both for erbium and zinc is much lower than one and decreases with growing dopant concentration in the melt (see the Table).

$K_{0eff} = f(C_L)$ and $C_S = f(C_L)$ curves for erbium and zinc in the $\text{LiNbO}_3:\text{Er}:\text{Zn}$ melt–crystal system are shown in Figure 2 and 3, respectively. Figure 3 also shows equivalent dependences for the $\text{LiNbO}_3:\text{Zn}$ system corresponding to the zinc concentration range in the melt

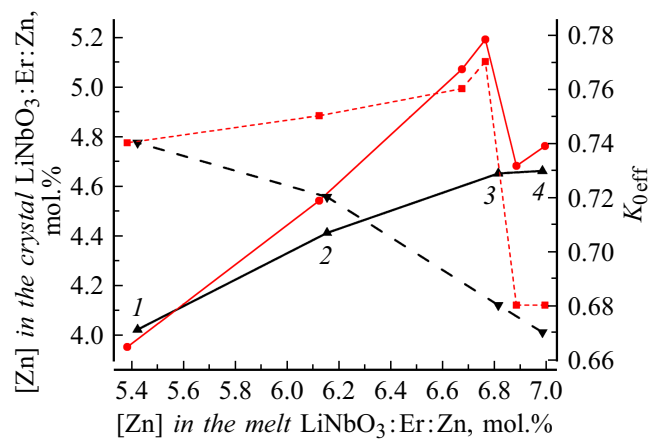


Figure 3. Dependences of Zn concentration (black solid line, triangles) and estimation distribution coefficient K_{0effZn} (black dashed line, triangles) in $\text{LiNbO}_3:\text{Er}:\text{Zn}$ crystals on Zn concentration in the melt. The numbers correspond to the single crystal Nos. (see the Table). Dependences of Zn concentrations (red solid line (in the online version), circles) and the estimation distribution coefficient K_{0effZn} (red dashed line (in the online version), squares) in $\text{LiNbO}_3:\text{Zn}$ crystals on Zn concentration in the melt [8,30].

within boundaries II ($C_{LZn} = 5.4\text{--}6.8$ mol.%) and III ($C_{LZn} > 6.8$ mol.%) according to [8,30].

A distinguishing feature of Er distribution in the $\text{LiNbO}_3:\text{Er}:\text{Zn}$ melt–crystal system is that the dopant concentration in single crystals throughout the test range is at the level of ≈ 0.5 mol.% (Figure 2, see the Table). However, almost the same, within the measurement error, Er concentrations in the $\text{LiNbO}_3:\text{Er}:\text{Zn}$ (№1 and 2) crystals grown from melts with Er concentration 0.79–0.81 mol.% and Zn concentration 5.42–6.15 mol.% are slightly higher than those in the $\text{LiNbO}_3:\text{Er}:\text{Zn}$ (№3 and 4) crystals grown from the $\text{LiNbO}_3:\text{Er}:\text{Zn}$ melts with Er concentration 0.82–0.85 mol.% and Zn concentration 6.81–6.98 mol.% (Figure 2, see the Table).

Dependence $C_{SZn} = f(C_{LZn})$ for the $\text{LiNbO}_3:\text{Er}:\text{Zn}$ melt–crystal system is monotonic (Figure 3). Zn concentra-

tion in crystals №1–3 grown from the $\text{LiNbO}_3:\text{Er}:\text{Zn}$ melt with $C_{\text{LZn}} = 5.42\text{--}6.81$ mol.% increases with increasing Zn concentration in the melt and remains unchanged in crystals №3 and 4 grown from the $\text{LiNbO}_3:\text{Er}:\text{Zn}$ melt with $C_{\text{LZn}} = 6.81\text{--}6.98$ mol.% (see the Table and Figure 3).

Zn distribution in the $\text{LiNbO}_3:\text{Er}:\text{Zn}$ melt–crystal system (Figure 3) differs dramatically from that in the $\text{LiNbO}_3:\text{Zn}$ system (Figure 3) not only due to the absence of sudden stepwise changes, but also due to the fact that $K_{\text{0effZn}} = f(C_{\text{LZn}})$ in the $\text{LiNbO}_3:\text{Zn}$ melt–crystal system is an increasing function in the melt concentration region 5.42–6.81 mol.%, while the Zn distribution coefficient in the $\text{LiNbO}_3:\text{Er}:\text{Zn}$ melt–crystal system is a decreasing function throughout the full test range (5.42–6.98 mol.%).

$\text{LiNbO}_3:\text{Zn}$ and $\text{LiNbO}_3:\text{Er}:\text{Zn}$ (№1) crystals grown from melts with Zn concentration close to the low concentration threshold $C_{\text{LZn}} = 5.36$ mol.% [8,30] have almost the same values of C_{SZn} and K_{0effZn} (Figure 3). With increasing Zn concentration in the melt due to increasing K_{0effZn} in the $\text{LiNbO}_3:\text{Zn}$ system and decreasing K_{0effZn} in the $\text{LiNbO}_3:\text{Er}:\text{Zn}$ system, difference in Zn concentrations occurs in $\text{LiNbO}_3:\text{Zn}$ and $\text{LiNbO}_3:\text{Er}:\text{Zn}$ crystals. Near the main concentration threshold $C_{\text{L}} = 6.8$ mol.% Zn (Figure 3, crystal №3), the difference in Zn concentrations is maximum. Then, due to sudden stepwise decrease of K_{0effZn} and C_{SZn} in the $\text{LiNbO}_3:\text{Zn}$ melt–crystal system (crystals in area III [8,30]), the difference in Zn concentrations in $\text{LiNbO}_3:\text{Zn}$ and $\text{LiNbO}_3:\text{Er}:\text{Zn}$ (№4) crystals becomes minimum (Figure 3).

It should be noted that the total concentration of Er and Zn dopants in $\text{LiNbO}_3:\text{Er}:\text{Zn}$ (№3, 4) crystals grown from the melts with Zn concentration 6.81 and 6.98 mol.%, respectively, is the same, equal to 5.16 mol.% and close to the Zn cation concentration in $\text{LiNbO}_3:\text{Zn}$ crystal (5.19 mol.%) grown from concentration area II (6.76 mol.% ZnO in the melt) [8,30]. This is an indirect evidence of „saturation“ of $\text{LiNbO}_3:\text{Er}:\text{Zn}$ (№3, 4) crystals with dopant cations (see the Table).

The experimental data shows that, when the $\text{LiNbO}_3:\text{Er}:\text{Zn}$ melt–crystal system is considered comprehensively, the Er concentration in crystals №1–4 within the measurement error is at constant level of ~ 0.5 mol.%. Zn concentration increases in crystals №1 and 2, while is constant in crystals №3 and 4, and does not depend on Zn concentration in the melt (see the Table, Figures 2 and 3).

$\text{LiNbO}_3:\text{Er}:\text{Zn}$ (№1–4) single crystals feature high degree of chemical homogeneity (see the Table). In addition, the express assessment of the number of scattering centers visualized in the single crystals in the presence of extended and point defects has shown that they are absent in all single crystals of the grown $\text{LiNbO}_3:\text{Er}:\text{Zn}$ series suggesting high optical purity of the material [29].

Optical homogeneity of grown $\text{LiNbO}_3:\text{Er}:\text{Zn}$ crystals was controlled by the laser conoscopy method. Conoscopic control of optical properties of lithium niobate crystals is a vivid and easy-to-access research method due the correlation between the conoscopic pattern type, structure

and properties and the crystal structure, optical properties and orientation as well as the presence of various types of defects in the crystal [34,35]. When crystals are irradiated with 1 mW emission, the recorded conoscopic patterns reflect the presence of defects in the crystal structure without the photorefraction effect. When 90 mW laser excitation is used, the conoscopic patterns show the intrinsic defects of the crystal that depend on its composition and growth conditions, as well as the defects induced by laser irradiation. Thus, the spatial distribution analysis of optical anomalies by the conoscopic method detects even minor changes in optical characteristics of the crystal in doping.

Conoscopic patterns of $\text{LiNbO}_3:\text{Er}:\text{Zn}$ (№1–4) crystals recorded by scanning on the input face plane using 1 mW and 90 mW laser emission are shown in Figure 4. The conoscopic patterns of $\text{LiNbO}_3:\text{Er}:\text{Zn}$ (№1, 2) crystals recorded at 1 mW laser emission have circular symmetry where the integrity of the black „Maltese cross“ is maintained in the center of the field of vision, and he isochromes look like concentric circles with the center in the optical axis emergence point (Figure 4, (1)–(4)). Laser scanning on the input face plane shows the presence of almost the same conoscopic patterns that are indicative of the optical homogeneity of the grown crystals by volume (Figure 4, (1)–(4)). This is the type of conoscopic patterns that demonstrates the optical homogeneity of samples. No additional distortions that occur when laser power is increased up to 90 mW are observed on the conoscopic patterns that indirectly proves that there is no photorefractive response from $\text{LiNbO}_3:\text{Er}:\text{Zn}$ crystals (№1, 2) (Figure 4, (9)–(12)).

Laser scanning results on the input face plane of $\text{LiNbO}_3:\text{Er}:\text{Zn}$ crystals (№3, 4) (Figure 4, (5)–(8) and (13)–(16)) differ from the results obtained for $\text{LiNbO}_3:\text{Er}:\text{Zn}$ crystals (№1, 2). For both $\text{LiNbO}_3:\text{Er}:\text{Zn}$ (№3, 4) crystals, two types of conoscopic patterns were obtained — those corresponding to uniaxial crystals (Figure 4, (5), (7), (13), (15)) and defective conoscopic patterns showing abnormal biaxiality (Figure 4, (6), (8), (14), (16)). Thus, by scanning on the input face plane of the studied $\text{LiNbO}_3:\text{Zn}:\text{Er}$ crystals conoscopic patterns were obtained that corresponded to the optically homogeneous crystals (crystals №1–4), and a set of defective conoscopic patterns with signs of abnormal optical biaxiality [32] corresponding to crystals №3 and 4.

The conoscopic patterns shown in Figures 4, (5), (7), (13), (15) have circular symmetry where the integrity of the black „Maltese cross“ is maintained in the center of the field of vision, and he isochromes look like concentric circles with the center in the optical axis emergence point. However, all conoscopic patterns of $\text{LiNbO}_3:\text{Er}:\text{Zn}$ (№3, 4) crystals show anomalies: the top right arm of the „Maltese cross“ has anomalies in the form of coupling of 1–2, 3–4, 5–6 isochromes (Figure 4, (5), (13)); in the form of distortions on all arms of the „Maltese cross“ (Figure 4, (7), (15)). Conoscopic patterns in Figure 4, (6), (8), (14), (16) contain insignificant signs of abnormal

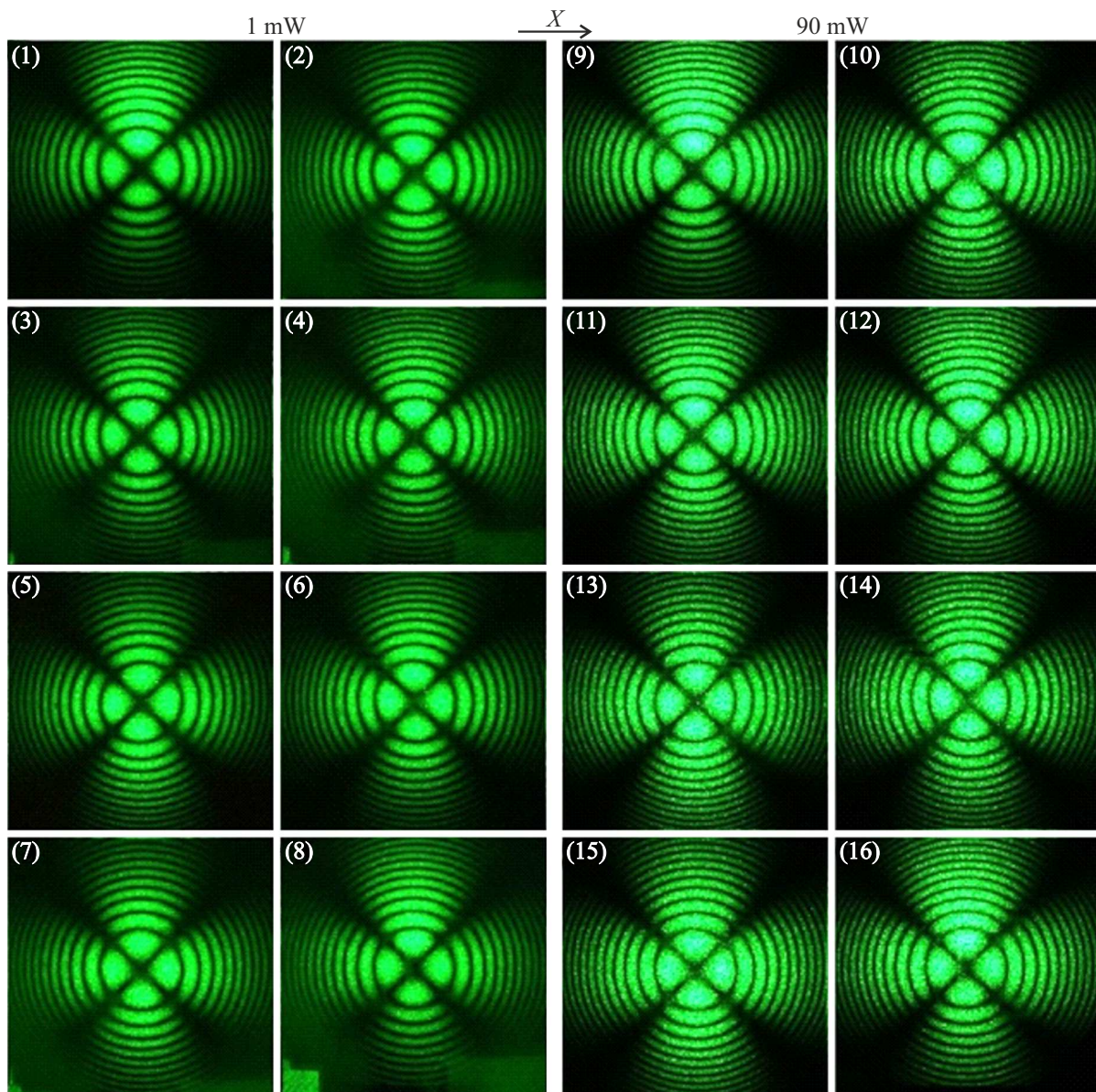


Figure 4. Conoscopic patterns of $\text{LiNbO}_3:\text{Er}:\text{Zn}$ crystals (№1 (1), (2), (9), (10), №2 (3), (4), (11), (12), №3 (5), (6), (13), (14), №4 (7), (8), (15), (16)) obtained at laser emission power 1 (1)–(8) and 90 (9)–(16) mW from 3 mm plates by scanning on the input face plane. The Z axis is perpendicular to the pattern plane. $\lambda = 532.0$ nm.

optical biaxiality when deformation occurs in the center of the black „Maltese cross“ in the form of displacement of the cross fragments (without separation) from the center in vertical direction corresponding to the optical indicatrix deformation direction of the crystal. Isochromes have slight ellipticity while maintaining a regular geometry (Figure 4, (6), (8), (14), (16)). The top left and bottom right arms of the „Maltese cross“ in the conoscopic pattern of $\text{LiNbO}_3:\text{Er}:\text{Zn}$ (№3) crystal have anomalies in the form of additional systems of interference bands (Figure 4, (6), (14)). For $\text{LiNbO}_3:\text{Er}:\text{Zn}$ (№4) crystal, additional anomalies are observed on the „Maltese cross“ arms in the right half-plane of the conoscopic pattern (Figure 4, (8), (16)).

Due to the fact that $\text{LiNbO}_3:\text{Er}:\text{Zn}$ (№3, 4) single crystals have high chemical homogeneity and do not have scattering centers [29] that proves the absence of extended and point defects in the crystal volume, conoscopic pattern distortions may be caused by the defective structure of $\text{LiNbO}_3:\text{Er}:\text{Zn}$ (№3, 4) crystals that results in local modification of elastic properties of the crystal and occurrence of mechanical stresses in it [32].

It is usual to describe the secondary (defective) structure of lithium niobate crystals in terms of a set of vacancy models [36,37]. In [26], the X-ray diffraction analysis of $\text{LiNbO}_3:[\text{Er} = 0.74 \text{ mol.}\%]$ crystal grown by the Czochralski method was used to show that Er^{3+} cations localize in the lithium octahedron of the structure ($\text{Er}_{\text{Li}}^{2+}$) and shift

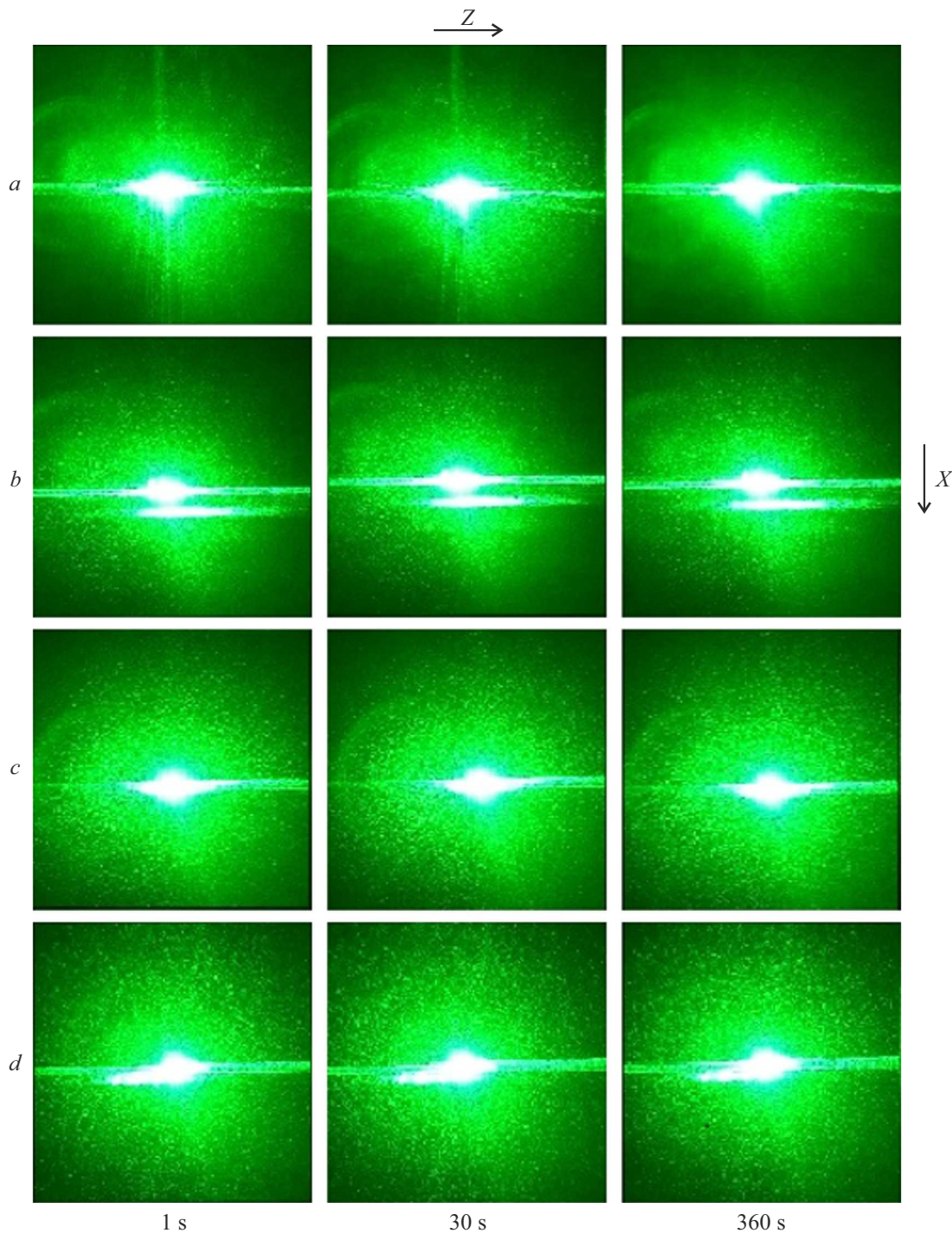


Figure 5. PLS patterns of $\text{LiNbO}_3:\text{Er}:\text{Zn}$ crystals ($N^{\circ}1$ (a), 2 (b), 3 (c), 4 (d)). $\lambda = 532.0 \text{ nm}$, $P = 160 \text{ mW}$.

towards its center, while the content of $\text{Nb}_{\text{Li}}^{4+}$ defects (deep electron traps — niobium cations localized in the lithium cation position [38]) tends to zero in this crystal. However, niobium cations were found in the crystal that were localized in the vacant octahedra of the crystal structure ($\text{Nb}_{\text{V}}^{5+}$ defect) and, consequently, vacancies in the niobium position ($\text{V}_{\text{Nb}}^{5-}$) were found [26]. Findings in [26] show that the niobium vacancy model is implemented [36,37,39] in

$\text{LiNbO}_3:[\text{Er} = 0.74 \text{ mol.}\%]$ studied crystal. Such features of the defective structure of $\text{LiNbO}_3:[\text{Er} = 0.74 \text{ mol.}\%]$ crystal [26] probably may be projected onto the features of the secondary structures of $\text{LiNbO}_3:\text{Er}:\text{Zn}$ crystals containing $\sim 0.5 \text{ mol.}\% \text{ Er}$.

According to [11,40,41], doping of the lithium niobate crystal with Zn cations up to the main threshold $\approx 7 \text{ mol.}\%$ (updated value according to [8,30] is equal to $6.8 \text{ mol.}\%$ in

the melt) results in considerable reduction of $\text{Nb}_{\text{Li}}^{4+}$ concentration due to their displacement by the doping cations with formation of $\text{Zn}_{\text{Li}}^{+}$. Crossing the main concentration threshold results in zinc cation introduction into the niobium octahedra of the crystal structure ($\text{Zn}_{\text{Nb}}^{3-}$) [11,40,41]. According to the X-ray diffraction analyses of $\text{LiNbO}_3:\text{Zn}$ crystals [8], $\text{Nb}_{\text{Li}}^{4+}$ defects are absent in the crystal grown from the melt with $[\text{Zn}] = 6.12 \text{ mol.}\%$ and occur in $\text{LiNbO}_3:\text{Zn}$ crystals when the doping component concentration is further increasing. Considering the above as well as almost unchanged ($\approx 0.5 \text{ mol.}\%$) Er concentration in $\text{LiNbO}_3:\text{Er}:\text{Zn}$ ($\text{N}^\circ 1-4$) crystals and growing concentration of Zn cations in them (see the Table), the number of $\text{Nb}_{\text{Li}}^{4+}$ defects in $\text{LiNbO}_3:\text{Er}:\text{Zn}$ ($\text{N}^\circ 1-4$) crystals may be assumed as minimized. However, the structure of $\text{LiNbO}_3:\text{Er}:\text{Zn}$ ($\text{N}^\circ 3, 4$) crystals probably undergoes „saturation“ with doping cations ($5.16 \text{ mol.}\%$) that may cause introduction of Zn cations in niobium octahedra of the crystal structure with formation of $\text{Zn}_{\text{Nb}}^{3-}$ defects. This hypothesis is also supported by the threshold ($6.8 \text{ mol.}\%$ [8,30]) zinc concentration in the melts from which $\text{LiNbO}_3:\text{Er}:\text{Zn}$ ($\text{N}^\circ 3, 4$) crystals were grown (see the Table). For $\text{LiNbO}_3:\text{Er}:\text{Zn}$ ($\text{N}^\circ 3, 4$) crystals, a complex self-compensation mechanism will be probably implemented involving $\text{Er}_{\text{Li}}^{+}$, $\text{Zn}_{\text{Li}}^{+}$, $\text{Nb}_{\text{V}}^{5+}$, $\text{Zn}_{\text{Nb}}^{3-}$, V_{Li}^{-} and $\text{V}_{\text{Nb}}^{5-}$, that resembles a self-compensation mechanism for $\text{LiNbO}_3:\text{Zn}$ crystals with the dopant concentration higher than the threshold concentration [11,41].

Thus, for $\text{LiNbO}_3:\text{Er}:\text{Zn}$ ($\text{N}^\circ 3, 4$) crystals, a concept of additive effect of doping elements (Er, Zn) and their concentration on the number and type of structural defects in the crystal may be implemented. This result is of high practical importance, because distribution of metal cations (intrinsic and doping) in the structure and their position in the octahedra define to a considerable extent ferroelectric and optical properties of LiNbO_3 crystals [2].

To investigate the PILS effect, the studied crystals were preliminary exposed to $\sim 160 \text{ mW}$ laser emission. Figure 4, (9)–(16) shows conoscopic patterns of $\text{LiNbO}_3:\text{Er}:\text{Zn}$ crystals at 90 mW laser power. For all examined crystals, no additional distortions were recorded in the conoscopic patterns that indirectly confirms the absence of photorefractive response of these crystals. Investigation of LiNbO_3 by the laser conoscopy method is in good agreement with the photoinduced light scattering data (Figure 5).

Figure 5 shows time dependences of the PILS patterns of $\text{LiNbO}_3:\text{Er}:\text{Zn}$ crystals. The view of the speckle structure of the PILS indicatrix is typical for lithium niobate crystals. Anyhow, for crystals with different composition grown by different methods, PILS speckle structure has its own thin features that may be used to investigate the crystal structure, micro- and macrohomogeneity. Figure 5 shows that, for the studied crystals even after exposure to 160 mW laser emission during 6 min, there is no photorefractive response, the PILS indicatrix is not expanded, and only circular scattering on static structural defects is observed.

Notwithstanding that Er is a colored impurity, Er introduction into the lithium niobate crystal does not result in the photorefractive effect. In terms of photorefractive properties, $\text{LiNbO}_3:\text{Er}:\text{Zn}$ crystals are close to the nominally pure crystals with identical composition. The PILS patterns remain unchanged throughout the experiment (Figure 5).

The photorefraction effect and photoinduced light scattering cause heavy destruction of the laser beam in the lithium niobate crystal and are interfering factors for emission generation and reconversion by the crystal [31]. Therefore the investigations intended to improve photorefractive properties of the lithium niobate crystal are essential for the development of materials with pre-defined specifications. The findings show that these lithium niobate crystals are promising as non-linear optical materials with low photorefraction effect and low PILS level.

Conclusion

Comprehensive investigations of $\text{LiNbO}_3:\text{Er}:\text{Zn}$ crystals containing $\sim 0.5 \text{ mol.}\%$ of Er and 4.02, 4.41, 4.65, 4.66 mol.% of Zn were carried out. All crystals studied herein have high chemical homogeneity: maximum deviation of doping component concentration along the growth axis of the studied crystals is $|0.05| \text{ mol.}\%$. For $\text{LiNbO}_3:\text{Er}:\text{Zn}$ crystals studied herein, there is no photorefractive response, the PILS indicatrix is not expanded, and only circular scattering on static structural defects is observed.

Crystals grown from the $\text{LiNbO}_3:\text{Er}:\text{Zn}$ ($0.79-0.85 \text{ mol.}\%$ Er, $5.42-6.98 \text{ mol.}\%$ Zn) melt have various degree of optical homogeneity. Laser conoscopy shows that $\text{LiNbO}_3:\text{Er}:\text{Zn}$ ($\text{N}^\circ 1$ and 2 crystals containing $\sim 0.5 \text{ mol.}\%$ Er, 4.02 and $4.41 \text{ mol.}\%$ Zn, respectively) feature high optical homogeneity, while $\text{LiNbO}_3:\text{Er}:\text{Zn}$ ($\text{N}^\circ 3$ and 4 crystals containing $\sim 0.5 \text{ mol.}\%$ Er, $\sim 4.65 \text{ mol.}\%$ Zn) have lower optical homogeneity. This may be attributed both to „saturation“ of $\text{LiNbO}_3:\text{Er}:\text{Zn}$ ($\text{N}^\circ 3$ and 4) crystals with dopant cations ($C_{\text{SEr}} + C_{\text{SZn}} = 5.16 \text{ mol.}\%$) and to Zn cation concentration in the melt that is equal to ($6.81 \text{ mol.}\%$, crystal $\text{N}^\circ 3$) and exceeds ($6.98 \text{ mol.}\%$, crystal $\text{N}^\circ 4$) the threshold concentration ($6.8 \text{ mol.}\%$ [8,30]). Thus, the optimum concentration ranges of the doping components in the initial melt for growing $\text{LiNbO}_3:\text{Er}:\text{Zn}$ ($\text{N}^\circ 1$ and 2) crystals, that have high chemical and optical homogeneity and optical damage resistance simultaneously, are equal to $0.79-0.81 \text{ mol.}\%$ Er and $5.42-6.15 \text{ mol.}\%$ Zn.

Funding

This study was supported financially by the Ministry of Science and Higher Education of the Russian Federation, research topic $\text{N}^\circ 0186-2022-0002$ (Reg.No.FMEZ-2022-0016).

Conflict of interest

The authors declare that they have no conflict of interest.

References

- [1] M.E. Lines, A.M. Glass. *Principles and Applications of Ferroelectrics and Related Materials* (Oxford, Clarendon, 1977)
- [2] Yu.S. Kuz'minov. *Elektroopticheskiy i nelineinoopticheskiy kristall niobata litiya* (Nauka, M., 1987) (in Russian).
- [3] T. Volk, M. Wohlecke. *Lithium Niobate. Defects, Photorefractive and Ferroelectric Switching* (Springer, Berlin, 2008)
- [4] C. Guanyu, L. Nanxi, D.N. Jun, L. Hong-Lin, Z. Yanyan, H.F. Yuan, Y.T.L. Lennon, Y. Yu, L. Ai-Qun, J.D. Aaron. *Adv. Photon.*, **4** (3), 034003 (2022). DOI: 10.1117/1.AP.4.3.034003
- [5] T. Tian, Y. Wen, L. Wei, S. Hui, Z. Yan, C. Yaoqing, M. Yunfeng, X. Jiayue. *J. Cryst. Growth.*, **565**, 126132 (2021). DOI: 10.1016/j.jcrysgro.2021.126132
- [6] H. Huangpu, C. Lutong, H. Hui. *Opt. Mater.*, **42**, 47 (2015). DOI: 10.1016/j.optmat.2014.12.016
- [7] O. Sánchez-Dena, C.D. Fierro-Ruiz, S.D. Villalobos-Mendoza, D.M.C. Flores, J.T. Elizalde-Galindo, R. Fariás. *Crystals*, **10** (11), 973 (2020). DOI: 10.3390/cryst10110973
- [8] M.N. Palatnikov, N.V. Sidorov, O.V. Makarova, I.V. Biryukova. *Fundamental'nye aspekty tekhnologii silno legirovannykh kristallov niobata litiya* (Izd-vo KNTs RAN, Apatity, 2017) (in Russian).
- [9] T. Volk, M. Wohlecke, N. Rubinina, A. Reichert, N. Razu-movski. *Ferroelectrics.*, **183** (1), 291 (1996). DOI: 10.1080/00150199608224116
- [10] N.V. Sidorov, M.N. Palatnikov, N.A. Tepliakova, I.V. Biryukova, R.A. Titov, O.V. Makarova, S.M. Masloboeva. *Monokristally niobata i tantalata litiya raznogo sostava i genezisa* (Izd-vo RAN, M., 2022)
- [11] N.V. Sidorov, T.R. Volk, B.N. Mavrin, V.T. Kalinnikov. *Niobat litiya: defekty, fotorefraksiya, kolebatelny spektr, polaritony* (Nauka, M., 2003) (in Russian).
- [12] M. Aillerie, P. Bourson, M. Mostefa, F. Abdi, M.D. Fontana. *J. Phys. Conf. Ser.*, **416**, 012001 (2013). DOI: 10.1088/1742-6596/416/1/012001
- [13] L. Kovács, L. Kocsor, É. Tichy-Rács, K. Lengyel, L. Bencs, G. Corradi. *Opt. Mater. Express.*, **9**(12), 4506 (2019). DOI: 10.1364/OME.9.004506
- [14] K. Lengyel, A. Peter, L. Kovacs, G. Corradi, L. Palfalvi, J. Hebling, M. Unferdorben, G. Dravec, I. Hajdara, Z. Szaller, K. Polgar. *Appl. Phys. Rev.*, **2** (4), 040601 (2015). DOI: 10.1063/1.4929917
- [15] V.Ya. Shur, A.R. Akhmatkhanov, I.S. Baturin. *Appl. Phys. Rev.*, **2** (4), 040604 (2015). DOI: 10.1063/1.4928591
- [16] L.A. Alioshina, A.V. Kadetova, O.V. Sidorova. *Trudy KNTs RAN: Materialovedeniye* **9**, 493 (2018) (in Russian). DOI: 10.25702/KSC.2307-5252.2018.9.1.493-498
- [17] M. Stoffel, H. Rinnert, E. Kokanyan, G. Demirkhanuan, H. Demirkhanuan, M. Aillerie. *Opt. Mater.*, **57**, 79 (2016). DOI: 10.1016/j.optmat.2016.04.013
- [18] C. Yang, X. Tu, S. Wang, K. Xiong, Y. Chen, Y. Zheng, E. Shi. *Opt. Mater.*, **105**, 109893 (2020). DOI: 10.1016/j.optmat.2020.109893
- [19] N. Mkhitarian, J. Zaraket, N. Kokanyan, E. Kokanyan, M. Aillerie. *EPJ Appl. Phys.*, **85**, 30502 (2019). DOI: 10.1051/epjap/2019180317
- [20] E.V. Stroganova, V.V. Galutskiy, N.N. Nalbantov, A.S. Kozin. *Optoelectronics, Instrumentation and Data Processing*, **53** (1), 77 (2017). DOI: 10.3103/S8756699017010113
- [21] P.L. Pernas, M.J. Hernandez, E. Ruiz, E. Cantelar, R. Nevado, C. Morant, G. Lifante, F. Cusso. *Appl. Surf. Sci.*, **161** (1–2), 123 (2000). DOI: 10.1016/S0169-4332(00)00147-1
- [22] Q. Yannan, W. Rui, X. Lili, X. Yanling, Y. Chunhui, L. Xinrong. *Cryst. Res. Technol.*, **46** (11), 1137 (2011). DOI: 10.1002/crat.201100254
- [23] Q. Yannan, W. Rui, X. Lili, X. Yanling, Y. Chunhui. *Opt. Commun.*, **285** (13–14), 2986 (2012). DOI: 10.1016/j.optcom.2012.02.066
- [24] T.R. Volk, V.I. Pryalkin, N.M. Rubinina. *Opt. Lett.*, **15** (18), 996 (1990). DOI: 10.1364/OL.15.000996
- [25] X. Zhen, R. Wang, W. Zheng, L. Zhao, Y. Xu. *Proc. SPIE: Optoelectronics, Materials, and Devices for Communications*, **4580**, 546 (2001). DOI: 10.1117/12.445013
- [26] M.N. Palatnikov, A.V. Kadetova, L.A. Aleshina, O.V. Sidorova, N.V. Sidorov, I.V. Biryukova, O.V. Makarova. *Opt. Laser Technol.*, **147**, 107671 (2022). DOI: 10.1016/j.optlastec.2021.107671
- [27] V. Bermudez, M.D. Serrano, J. Tornero, E. Dieguez. *Solid State Commun.*, **112** (12), 699 (1999). DOI: 10.1016/S0038-1098(99)00419-6
- [28] X.H. Zhen, W.S. Xu, C.Z. Zhao, L.C. Zhao, Y.H. Xu. *Cryst. Res. Technol.*, **37** (9), 976 (2002). DOI: 10.1002/1521-4079(200209)37:9<976::AID-CRAT976>3.0.CO;2-F
- [29] I.N. Efremov, I.V. Biryukova, O.E. Kravchenko, M.N. Palatnikov. *Trudy KNTs RAN. Seriya: Tekhnicheskie nauki*, **13** (90), 2022 (2010) (in Russian). DOI: 10.37614/2949-1215.2022.13.1.015
- [30] M.N. Palatnikov, I.V. Biryukova, O.V. Makarova, V.V. Efremov, O.E. Kravchenko, V.I. Skiba, N.V. Sidorov, I.N. Efremov. *Inorg. Mater.*, **51** (4), 375 (2015). DOI: 10.1134/S0020168515040123
- [31] M.N. Palatnikov, V.A. Sandler, N.V. Sidorov, I.N. Efremov, O.V. Makarova. *Instrum. Exp. Tech.*, **63** (3), 383 (2020). DOI: 10.1134/S0020441220040089
- [32] N.V. Sidorov, O.Yu. Pikul', N.A. Teplyakova, M.N. Palatnikov. *Lazernaya konoskopiya i fotoindutsirovannoe rasseyanie sveta v issledovaniyakh svoystv nelineyno-opticheskogo monokristalla niobata litiya* (RAN, M., 2019) (in Russian).
- [33] V.A. Maksimenko, A.V. Syuy, Yu.M. Karpets. *Fotoindutsirovannyye protsessy v ktistallakh niobata litiya* (Fizmatlit, M., 2008) (in Russian)
- [34] K.A. Rudoï, V.I. Stroganov, L.V. Alekseeva, B.V. Nabatov, A.F. Konstantinova, E.A. Evdishchenko, B.I. Kidyarov. *Crystrallogr. Rep.*, **48** (2), 300 (2003). DOI: 10.1134/1.1564211
- [35] O.Y. Pikoul. *J. Appl. Crystallogr.*, **43**, 955 (2010). DOI: 10.1107/S0021889810022375
- [36] N. Zotov, H. Boysen, F. Frey, T. Metzger, E. Born. *J. Phys. Chem. Solids*, **55** (2), 145 (1994). DOI: 10.1016/0022-3697(94)90071-X
- [37] O. Sánchez-Dena, S.D. Villalobos-Mendoza, R. Fariás, C.D. Fierro-Ruiz. *Crystals*, **10** (11), 990 (2020). DOI: 10.3390/cryst10110990
- [38] D.M. Smyth. *Ferroelectrics*, **50** (1), 93 (1983). DOI: 10.1080/00150198308014437

- [39] G.E. Peterson, A. Carnevale. J. Chem. Phys., **56** (10), 4848 (1972). DOI: 10.1063/1.1676960
- [40] T.S. Chernaya, B.A. Maksimov, T.R. Volk, N.M. Rubinina, V.I. Simonov. JETP Lett., **73** (2), 103 (2001). DOI: 10.1134/1.1358430
- [41] T.R. Volk, B. Maximov, T. Chernaya, N. Rubinina, M. Wohlecke, V. Simonov. Appl. Phys. B-Lasers O., **72** (6), 647 (2001). DOI: 10.1007/s003400100548

Translated by Ego Translating